

An application of Saddlepoint Approximation for period detection of stellar light observations

Efthymia Derezea¹, Alfred Kume¹, Dirk Froebrich²

November 21, 2022

1. *School of Mathematics, Statistics and Actuarial Science, University of Kent, Canterbury CT2 7FS, UK*
2. *School of Physical Sciences, University of Kent, Canterbury CT2 7NH, UK*

Abstract

One of the main features of interest in analysing the light curves of stars is the underlying periodic behaviour. The corresponding observations are a complex type of time series with unequally spaced time points. The main tools for analysing these type of data rely on the periodogram-like functions, constructed with a desired feature so that the peaks indicate the presence of a potential period. In this paper, we explore a particular periodogram for the irregularly observed time series data. We identify the potential periods by implementing the saddlepoint approximation, as a faster and more accurate alternative to the simulation based methods that are currently used. The power analysis of the testing methodology is reported together with applications using light curves from the Hunting Outbursting Young Stars citizen science project.

Key words: Cross-Validation, Hypotheses testing, Non-parametric statistics, Periodogram, Quadratic Forms, Saddlepoint

1 Introduction

The problem of estimating the periodicity of time series in the presence of irregularly sampled data appears in many disciplines including Economics (see Baltagi, Wu (1999)), Climatology (see Schulz, Statterger (1997)), Biology (see Heerah et al. (2020)), or Astronomy (for example for rotation period searches of stars as in Herbst et al. (2007); Bouvier et al. (2014)). In this paper, we focus on astronomical light curves of stars, whose observations represent brightness measurements over time. Current and future large astronomical surveys potentially generate millions of such light curves. Thus, there is a need of accurate, automated, and fast methodologies to determine periods reliably. Depending on the type of star, being able to estimate the period of light curves can provide important information about the star itself (rotation period), its formation, its internal structure and the environment it is in (e.g. structures in accretion disks around young stars).

The sampling of light curves occurs at irregular time points because the data collection which is carried out by ground telescopes can be affected by many factors such as weather, visibility or the telescope's schedule. The data represents the brightness of stars, which are usually quoted in magnitudes y . These are determined from the physical flux measurements f as $y = -2.5 \log(f/f_0)$, where f_0 is the flux zero point. Thus, numerically large magnitude values indicate fainter brightness and vice versa. The times for the data points in the light curves are usually registered as a Julian date. This is a count of days since noon January 1st, 4713 BC. A typical time series of this type is shown in Figure 5 (Left). Note that, each data point has an associated individual measurement accuracy (see the grey bars centered at the observation

points there), small values of which reflect small measurement uncertainty. These uncertainties represent one sigma errors and are determined during the data processing and calibration of the astronomical images.

Let \mathbf{y} denote the vector of n signal observations such that each entry y_j is the data arriving in a non systematic way at times t_j , $j = 1, \dots, n$. We assume the data are generated as

$$y_j = g(t_j; p) + \epsilon_j \quad (1)$$

where g is the assumed true function with period p while $\epsilon_j \sim N(0, \sigma^2)$ are the measurement errors. If we take the measurement accuracies, which we will denote as s_j , into account, (1) changes to $y_j/s_j = g(t_j; p)/s_j + \epsilon_j$ as a weighted regression model.

The main objective is to perform statistical inference about the period p but the challenge is two fold: the first being the estimation of the period p and the second that of associating some credibility to the claim that the data is indeed periodic. The former problem is addressed by many papers which deal with direct estimation of p but the latter, which is the motivation of the work reported here, is either not paid full attention or done in computationally inefficient ways. Depending on the model of interest, a common strategy for the period estimation is based on the optimal entry of some periodogram function. The period estimation based on linear regression, reported in Thieler et al. (2013), uses a periodogram function which essentially reflects the regression goodness of fit for each candidate period and the accepted value of p is that for which the best regression fit is attained. Along the same principle of least square estimation, Hall et al. (2000) use non-parametric models for identifying the optimal p . Obviously, non-parametric approaches make less assumptions about the shape of the light curves, an example of which is the Gaussian process regression (GPR) as seen in Wang et al. (2012).

Please note that, when the term ‘‘periodogram’’ is used, we refer to a broad range of discrete functions defined on a grid of possible period values. Extreme periodogram values (high or low peaks depending on the periodogram chosen) naturally point to potentially valid periods. Figure 4 (Right) displays a periodogram (based on the standard F-statistic which we will discuss in Section 3), for a real light curve with period at 2.1763 days as in Froebrich et al. (2021). There are many approaches for constructing periodograms depending on the models of interest. The focus of this paper will be mainly on these non-parametric models and their extensions, such as accounting for correlated residuals and using the additional measurement accuracies in the form of weights.

We are particularly interested in addressing here whether a particular peak of the periodogram represents correctly a valid period and is not just an artifact produced by noisy data. Usually this is addressed by associating p-values and/or performing appropriate hypothesis testing. While this problem is well understood for methods depending on linear models and least squares regression, it is not straightforward how to obtain these p-values when non-parametric regression is used. This is certainly the case for the period detection for irregularly observed time series. For example, in Wang et al. (2012), the authors specifically state that a formal test is needed to decide on the validity of a proposed period under such schemes. In this paper, we provide accurate tests to be implemented under such settings, as a faster alternative to the simulation based approaches that are implemented as in Do et al. (2009) for example. A computationally efficient alternative is important given the large amount of data available. Our method improves drastically the calculation time when GPR models are used by performing the calculations in 2% of the time needed for doing the same analysis using Monte Carlo. For more details on time comparisons see Table 4 in Appendix A.1. In particular, we introduce a general Hypothesis test setting for non-parametric models and specifically Gaussian process regression, providing thus a solution to the problem of period detection for these flexible models. Furthermore, we show how these tests can be adjusted in the presence of correlated noise (red noise), obtaining this way more accurate results while drastically reducing the number of periods which could be falsely identified as valid.

Specifically, in this paper we focus on a hypothesis testing approach for a range of models for periodogram construction, including those derived from non-parametric estimation methods. In order to carry out our period estimation for irregularly sampled time series, we will use the generalised F-statistics (7) to construct the entries of periodogram functions and use the saddlepoint approximation method to evaluate the corresponding p-values for the potential periods. Our method is reported here for period detection in three sets of models:

- Non-parametric models. This is particularly useful when non-parametric regression (including non-ordinary least squares regression) is used and is shown to be at least as good as the computationally demanding simulation alternatives.
- Gaussian Process Regression. In particular the leave-one-out cross validation measure used for model fitting leads to the test statistics of a similar quadratic form.
- Correlated background noise. These models are extensions of those above while red noise correlation structure is assumed. The saddlepoint method for the resulting quadratic forms has a similar form.

The outline of the paper is as follows. Current methods and related work are discussed in Section 2. In Section 3 we introduce the general framework of the Hypothesis testing. We see how this framework can be expanded for non-parametric models in Section 3.1. In Section 3.2 we introduce a test based on leave-one-out cross validation error for Gaussian process regression models and in Section 3.3 we discuss the natural extension of the above mentioned tests under the presence of correlated noise. Specifics on implementation of the Saddlepoint approximation are provided in Section 4. The tests' performance will be assessed through a detailed power analysis in Section 5, real light curve applications are examined in Section 6, and finally in Section 7 there is a discussion about future work and conclusions.

2 Current methods and related work

For the general case of equally spaced time observations the classical periodogram is the estimator of our signal's spectral density:

$$P(\omega) = \left| \int g(t) e^{-2\pi i \omega t} dt \right|^2 \quad (2)$$

where ω is the frequency (it holds that $\omega = 1/p$). There are many approaches based on the classical periodogram, see for example Schuster (1898).

These methods however fail when our observations do not arrive at regular intervals. An illustrative discussion regarding this can be found in VanderPlas (2018), where the author shows how an irregular sampling can lead to a noisy Fourier Transform and thus to noisy estimations of the Spectral density. A popular approach dealing with this problem is that based on the Lomb-Scargle (LS) periodogram (Scargle, 1982) which is a generalized form of the classical periodogram (2) but is not affected by irregular time spacing. It can be shown that this method produces identical results to that obtained by fitting a single sinusoidal wave using the ordinary least squares regression while assessing the fit at each period using the squared error, (Lomb (1976); VanderPlas (2018)). The model fitted is basically the same as that of (3) below but without the intercept term. This model is also studied in Reimann (1994) where the author explores the asymptotic behaviour of the maximum likelihood estimator (MLE) of the frequency ω and proves its consistency based on some regularity conditions regarding the residuals distribution and certain assumptions based on the distribution of time points t_j . The author shows that the classic periodogram

(moment) estimator of frequency has a larger asymptotic variance than that of the MLE. A very popular model used for the stellar light curves is that based on the sinusoidal functions:

$$y_j = \beta_0 + \beta_1 \sin(2\pi t_j/p) + \beta_2 \cos(2\pi t_j/p) + \epsilon_j \quad (3)$$

see for example Cumming et al. (1999) or VanderPlas, Ivezić (2015). These models are clearly very special cases of (1) while there exist many other approaches based on various forms for the periodic function g . For example, Akerlof et al. (1994) fit cubic b-splines using least squares regression in order to estimate the periods of various stars. Another example, is the use of periodic splines as seen in Oh et al. (2004), where the authors use cubic splines with a periodic restriction to fit the model by performing robust regression (i.e. Huber’s regression) and finally the fit is assessed based on a cross validation approximation. For more general robust regression settings, see for example Katkovnik (1998), where the coefficients of a sinusoidal wave are estimated using Huber’s M-regression. A detailed discussion to that end can be found in Thieler et al. (2013) where the authors study, under the same framework, periodograms obtained by combinations of models (such as splines or sinusoidal basis) and different types of regression. In a comprehensive simulation study they compare the performance of the methods for light curves with/without the presence of red noise and show, for example, that robust regression methods are more reliable for data with outliers.

A straightforward application of the simple linear regression method for fitting model (3) for various values of p leads to the construction of some periodogram function whose entries are calculated according to the coefficient of determination R^2 . The valid periods are expected to generate the highest R^2 values and hence focusing on the peaks of such periodogram functions is a sensible approach. Additionally, since R^2 has a known Beta distribution (see e.g. Schwarzenberg-Czerny (1998)) under the null assumption (of no signal in the data for example) the associated p-values for each potential period reflect the confidence for each proposed period. A similar approach is used in the current literature as in Thieler et al. (2013) where the proposed periods correspond to the highest peaks of the R^2 statistics for which the corresponding p-values were low. In that paper the authors calculate the corresponding p-values by fitting to the obtained periodogram a Beta distribution using the Cramér-von Mises distance.

Specific interest is shown in period detection under the presence of red noise. The assumed correlation structure of red noise coincides with that of an AR(1) process if the observations are collected at equally spaced time observations, see e.g. Von Storch, Zwiers (2001). In these cases of AR(1) errors, (not of our primary interest here), Benlloch et al. (2001) identified valid periodogram peaks against red background noise using Monte Carlo methods. Later some exact tests were developed, see for example Vaughan (2005). In the case of unequally spaced time series however most of the corresponding methods used are based on Monte Carlo approaches in order to identify the valid periods in the presence of a red background noise, for example Zhou, Sornette (2002).

Other approaches in the literature for period estimation are based on flexible non-parametric models making less assumptions about the shape of the function g . A typical example is the use of kernel smoothing regression as studied in great depth in Hall et al. (2000), where the estimates for \hat{g} are obtained using the Nadaraya-Watson estimator for a given period and assuming some kernel function. Note that for any given p the parameters of g are immediately obtained based on the minimal sum of squared errors. Hence a grid search on p is sufficient to obtain \hat{p} as well as the parameter estimates of g . One could think of the corresponding periodogram function here comprising of values of sums of squared errors for various p . The authors provide the asymptotic behaviour of their optimal period estimator \hat{p} and show that it is consistent under certain conditions and converges to the true parameter with an $O(n^{-1/3})$ rate. Gaussian process regression for this problem is considered in Wang et al. (2012). A prior over functions g is assumed to follow a Multivariate Normal distribution $\mathbf{g} \sim N(\mathbf{0}, \mathbf{K})$, where \mathbf{K} is an $n \times n$ covariance matrix in our case,

with entries calculated according to (4)

$$\mathbf{K}_{jk} = K(t_j - t_k) = A \exp(-2 \sin^2(\frac{\pi}{p}(t_j - t_k))/h^2) \quad j, k = 1, 2, \dots, n \quad (4)$$

and A denoting the amplitude, p the period and h a smoothing parameter. It can be shown that for each candidate period p the corresponding posterior distribution of the fitted function \mathbf{g} at the time points t_j is Multivariate Normal, with mean and covariance:

$$E(\mathbf{g}) = \mathbf{W}\mathbf{y} \quad \text{Cov}(\mathbf{g}) = \mathbf{K} - \mathbf{W}\mathbf{K} \quad (5)$$

where $\mathbf{W} = \mathbf{K}[\mathbf{K} + \sigma^2\mathbf{I}]^{-1}$ and with σ^2 we denote the variance of our observations.

The parameters are estimated from the marginal likelihood for a given particular period p and similar to pseudo-likelihood methodology the optimal p is chosen to be the maximizer of the resulting marginal likelihood (see more details in Section 3.3). Note that if individual measurement accuracies s_j are to be taken into account, a simple update is needed for using a weighted Gaussian process regression model with, $\mathbf{W} = \mathbf{K}[\mathbf{K} + \mathbf{Q}^{-2}\sigma_n^2\mathbf{I}]^{-1}$ where \mathbf{Q} is a diagonal matrix with the weights $q_j = 1/s_j$ in its diagonal. The authors in Wang et al. (2012) claim that their method outperforms that of LS periodogram for data that deviate from the sinusoidal assumption. They also emphasise that a formal statistical test is needed to determine whether the estimated/proposed period can be considered valid. In this paper, we propose a test based on pseudo-likelihood arguments leading to ratios of quadratic forms for normally distributed terms. As the corresponding distributions are not readily available in closed form, a saddlepoint approximation is implemented and is shown to work well in a range of similar models applied for period estimation.

3 Hypothesis testing for period detection

As seen in Section 1 the focus of this paper is determining whether a periodogram peak represents a valid period. The common approaches to this problem are based on running hypothesis tests sequentially and relating them to some periodogram entries. Each periodogram entry could be the value of a chosen goodness of fit test statistic in our case, and we use the corresponding p-value to construct the hypothesis testing whether the given statistics are generated from just noise or period bearing data. In other words, the peaks in the corresponding periodogram point to those candidate periods p which are the most likely to generate the data and their corresponding magnitude of the p-values of the goodness of fit statistics indicate their associated credibility. The idea of sequential hypothesis testing for each candidate period p is summarized as follows:

$$\begin{aligned} H_0 : \mathcal{M}_0 \text{ model, no signal in the data} \\ \text{vs} \\ H_1 : \mathcal{M}_1 \text{ model with signal of period } p \end{aligned} \quad (6)$$

This strategy is adopted by the astronomy literature as in Schwarzenberg-Czerny (1998), where the distribution under the assumption of model \mathcal{M}_0 is derived for empirical periodograms like LS. In many papers the sequential hypothesis testing is based on simulating data according to H_0 as seen in Do et al. (2009) and then comparing their empirical distribution to the observed values of the periodogram peaks.

Note that these tests belong to the general family of pseudo-likelihood ratio tests that are based on the relative performance of both models \mathcal{M}_0 and \mathcal{M}_1 . This approach is in fact similar to that applied to the standard model selection in linear regression for nested models. Similar use is seen in time series analysis as shown in Berenblut, Webb (1973) where the authors compare a simple linear model to that

with additional AR(1) errors and the resulting statistic is related to that of Durbin, Watson (1950). More specifically, they show that in this context the one sided hypothesis testing is approximately UMP, see also Paoletta (2018) for an interesting discussion to that end. In non-parametric regression as seen in Azzalini, Bowman (1993) a similar test is used for testing the linearity assumption in the data versus non linear models \mathcal{M}_1 produced by kernel smoothing regression or spline function families.

Note that similar to the standard F-tests used in the linear regression, the associated test statistics for the above mentioned tests are in fact constructed as ratios of residual sums of squares which correspond to quadratic forms of zero mean normal components. The added difficulty including our models of interest is that for each candidate p , the terms in the numerator and denominator of those ratios are not necessarily independent. Hence, the standard F-test statistics can not be generally applied. A typical example is that in timeseries for nested ARMA models where standard results for the F-test no longer apply. This dependence is not fully addressed in the context of this particular problem. Typically simulation based approaches are implemented to overcome such difficulties.

In our context, we will perform hypothesis testing as in (6) such that the corresponding model for \mathcal{M}_0 would be just a constant, namely no periodic behavior in the data i.e. the light curve is just noise. This is equivalent to the model (3) reducing to the intercept term β_0 . On the other hand, if there was a periodic signal, the test will suggest as appropriate the alternative fitted models \mathcal{M}_1 that will contain the periodic terms as in (3) (or a more general form as in non-parametric regression). As a result, the stronger the evidence of departure from \mathcal{M}_0 towards \mathcal{M}_1 for some period p , the stronger the claim that this period is present in the signal. Note that a natural goodness of fit measure among various regression models is based on comparing the residual sums of squares RSS_0 and RSS_1 for the null and alternative models as:

$$F = \frac{(RSS_0 - RSS_1)}{RSS_1} = \frac{\mathbf{y}^\top \mathbf{M}_0 \mathbf{y} - \mathbf{y}^\top \mathbf{M}_1 \mathbf{y}}{\mathbf{y}^\top \mathbf{M}_1 \mathbf{y}} \quad (7)$$

with matrices \mathbf{M}_0 and \mathbf{M}_1 depending on the models of interest. In order to perform hypothesis testing, we need to evaluate the distribution of F , namely $P(F \leq f)$ under the null hypothesis. One can easily show that if $\mathbf{M}_0 = \mathbf{I} - \mathbf{1}\mathbf{1}^\top/n$ is some centering matrix with $\mathbf{1}$ denoting the column vector of ones,

$$P(F > f) = P(\hat{\boldsymbol{\epsilon}}^\top (\mathbf{I} - (1 + f)\mathbf{M}_1) \hat{\boldsymbol{\epsilon}} > 0) \quad (8)$$

where \mathbf{I} is the $n \times n$ identity matrix and $\hat{\boldsymbol{\epsilon}} = \mathbf{M}_0 \mathbf{y}$. If we replace f in (8) with a specific observed value of our statistic, e.g t_{obs} , the probability $P(F > t_{obs})$ is the p-value for our generalised F-test.

Some remarks on the ordinary F-statistics for linear regression

In the case of ordinary linear regression (3) a periodic structure is assumed and the statistic (7), if appropriately scaled, coincides with the ordinary F-statistics. The rescaling constant $c = \frac{n-m_1}{m_1-m_0}$ depends on the respective numbers of parameters m_0 and m_1 for models \mathcal{M}_0 and \mathcal{M}_1 . Namely, under the null assumption of white noise, the statistics

$$F \cdot c \sim F(m_1 - m_0, n - m_1) \quad (9)$$

with the numerator and denominator terms of (7) being independent random variables following chi-square distributions with $m_1 - m_0$ and $n - m_1$ degrees of freedom. Here, $\mathbf{M}_0 = \mathbf{I} - \mathbf{1}\mathbf{1}^\top/n$ is a fixed centering matrix, $\mathbf{M}_1 = \mathbf{I} - \mathbf{X}(\mathbf{X}^\top \mathbf{X})^{-1} \mathbf{X}^\top$ with \mathbf{X} being the design matrix of our model depending on observation time points. Note that from the standard calculations of the projection matrix $\mathbf{P} = \mathbf{X}(\mathbf{X}^\top \mathbf{X})^{-1} \mathbf{X}^\top$ in regression we can easily see that $\mathbf{M}_1 = (\mathbf{I} - \mathbf{P})^\top (\mathbf{I} - \mathbf{P}) = \mathbf{I} - \mathbf{P}$ and in particular the vector $\mathbf{1}$ is in the null space of \mathbf{M}_1 . This implies that $\mathbf{y}^\top \mathbf{M}_1 \mathbf{y}$ is invariant of the intercept in the model \mathcal{M}_0 and therefore

the statistic (7) is not affected if the data points \mathbf{y} are centralised, namely replaced by residual vector $\hat{\boldsymbol{\epsilon}} = \mathbf{M}_0\mathbf{y}$. Note that under this setting, the eigenvalues of \mathbf{M}_1 can be either zero or one and that is why (9) holds. The corresponding p-values are immediately available from standard packages like R.

In situations where more general alternatives are explored for \mathcal{M}_1 , the structure of \mathbf{M}_1 does not lead to the standard F-distribution for the statistic (7) and hence it is not straightforward to obtain its p-values. Naive Monte Carlo methods are adopted for these cases, and have been extensively used in the relevant literature such as Do et al. (2009) and Halpern et al. (2003), where for each trial period say p , many noise curves are simulated and the corresponding p-value is estimated based on the corresponding empirical distribution of the F-statistic (or something equivalent). In fact, we can show that for these cases there is no need to run simulations as the p-values are easily evaluated using the saddlepoint approximation explained in Section 4.

3.1 Generalized F-test for non-parametric periodograms

In this section we consider more complicated models \mathcal{M}_1 to describe our alternative hypothesis and see how the F-statistic as seen in (7) can be used for non-parametric settings such as kernel or Gaussian process regression (and in general for any linear smoother). The statistic (7) has been used in Azzalini, Bowman (1993) as a linearity test, where a comparison was conducted between a linear and a non-parametric model.

By following the same idea, we compare a constant (as the null model) with a non-parametric model for a given period. Under this setting, while the centering matrix $\mathbf{M}_0 = \mathbf{I} - \mathbf{1}\mathbf{1}^\top/n$ remains the same, $\mathbf{M}_1 = (\mathbf{I} - \mathbf{W})^\top(\mathbf{I} - \mathbf{W})$ is not a projection matrix, since \mathbf{W} is a $n \times n$ matrix depending on the observation times and additional model parameters as seen in (5) and (4).

The appropriate period detection test of the optimal periodogram entries requires the evaluation of the distribution of F under the null hypothesis, which due to \mathbf{M}_1 can no longer be assumed to follow a standard F distribution. We should note again that this test is also depending on the alternative model through \mathbf{M}_1 . The probability $P(F > t_{obs})$ of interest, is given by (8) and thus the problem reduces to that of evaluating these values for the distribution of such Quadratic form of some normally distributed terms.

3.2 CVF-test for Gaussian process regression

In the previous section we discussed how the generalised F-test can be used to create the corresponding periodogram for detecting valid periods when \mathcal{M}_1 is some non-parametric model and the resulting matrix \mathbf{M}_1 is not a projection matrix any more. Here we look specifically at the explicit expressions for \mathbf{M}_1 when the non-parametric model used is the Gaussian process Regression (GPR) and the natural goodness of fit measure based on cross-validation score is used. As seen in Section 2, in order to estimate the parameters for the GPR model (including the period), we can either maximize the marginal likelihood or minimize the cross-validation error. We can build a statistic/periodogram based on the leave-one-out cross-validation error

$$CVE = \sum_{j=1}^n (y_j - g_{-j}(t_j))^2 \quad (10)$$

and can use this measure for comparing the predictive ability of the GPR model at period p with that of the mean \mathcal{M}_0 . As seen in Williams, Rasmussen (2006), each term in (10) can be simplified to

$$y_j - g_{-j}(t_j) = \frac{[(\mathbf{K} + \sigma_n^2\mathbf{I})^{-1}\mathbf{y}]_j}{[(\mathbf{K} + \sigma_n^2\mathbf{I})^{-1}]_{jj}} \quad (11)$$

and in the vectorized form these entries are shown to be $\mathbf{y}^\top(\mathbf{K} + \sigma_n^2\mathbf{I})^{-1}\mathbf{B}_2$ where \mathbf{B}_2 is a diagonal matrix,

such that d_j is the j th diagonal element of the inverse of the matrix $\mathbf{K} + \sigma_n^2 \mathbf{I}$, namely, $d_j = \text{diag}((\mathbf{K} + \sigma_n^2 \mathbf{I})^{-1})_j$. Therefore, by denoting as $\mathbf{B} = (\mathbf{K} + \sigma_n^2 \mathbf{I})^{-1} \mathbf{B}_2$, we can write CVE as a quadratic form in \mathbf{y} as

$$CVE = \sum_{j=1}^n \left(\frac{[(\mathbf{K} + \sigma_n^2 \mathbf{I})^{-1}]_j}{d_j} \right) \cdot y_j)^2 = \mathbf{y}^\top \mathbf{B} \mathbf{B}^\top \mathbf{y} \quad (12)$$

In the same spirit as that of (7), a similar goodness of fit statistic based on the cross validation errors for the null model and that for a particular g choice using GPR is given below as:

$$CVF = \frac{CVE_0 - CVE_1}{CVE_1} = \frac{\sum_{j=1}^n (y_j - y_{-j}^-)^2 - \sum_{i=j}^n (y_j - g_{-j}(t_j))^2}{\sum_{j=1}^n (y_j - g_{-j}(t_j))^2} \quad (13)$$

where y_{-j}^- denotes the j^{th} leave-one-out mean. It can be easily shown that the CVF-statistic can be written in the form of (7) where $\mathbf{M}_1 = \mathbf{B} \mathbf{B}^\top$ and $\mathbf{M}_0 = \mathbf{M} \mathbf{M}^\top$, is a matrix used for the leave one out mean terms, with 1 in the diagonal and $-\frac{1}{n-1}$ everywhere else. The problem again reduces to that of estimating a simple Normal Quadratic form, and Saddlepoint approximation can be implemented in order to obtain fast and accurate results.

3.3 Testing in the presence of correlated red noise

In this section we consider the situation when a particular correlated noise (red noise) structure is assumed for residual terms ϵ . Let us assume for example that the correlation structure between any pair of residuals observed at a single time unit apart is, $\text{Corr}(\epsilon_j, \epsilon_{j-1}) = \rho$ for any j and some $\rho \in (-1, 1)$. This in turn implies that $\text{Corr}(\epsilon_j, \epsilon_{j-2}) = \rho^2$ and in general for any pair of residuals observed at time units t_j and t_k , $\text{Corr}(\epsilon_{t_j}, \epsilon_{t_k}) = \rho^{|t_j - t_k|}$. The red noise terms are distributed as:

$$\boldsymbol{\epsilon} \sim N(0, \sigma^2 \mathbf{C}_\rho) \quad \text{where} \quad \mathbf{C}_\rho = \begin{bmatrix} 1 & \rho^{|t_1 - t_2|} & \rho^{|t_1 - t_3|} & \dots & \rho^{|t_1 - t_n|} \\ & 1 & \rho^{|t_1 - t_2|} & \vdots & \rho^{|t_2 - t_n|} \\ \vdots & & & \ddots & \\ & & & & \dots & 1 \end{bmatrix} \quad (14)$$

Note that matrix \mathbf{C}_ρ takes into account the irregularly sampled nature of the data, such that the correlation between the observations depends on their time distance, the further away two points, the less the correlation assumed for the corresponding residuals. If $\rho = 0$, $\mathbf{C}_\rho = \mathbf{I}$ then the model reduces to that of the white noise. In order to calculate (7) for various p , we need to estimate the model parameters of \mathcal{M}_1 . This, for the case of GPR, is achieved by maximizing the marginal likelihood or alternatively by minimizing the leave-one-out cross-validation error. Under the presence of red noise, the marginal likelihood for GPR is:

$$\log P(\mathbf{y}|A, h, \sigma^2, \rho) = -\frac{1}{2} \mathbf{y}^\top (\mathbf{K} + \sigma^2 \mathbf{C}_\rho)^{-1} \mathbf{y} - \frac{1}{2} \log |\mathbf{K} + \sigma^2 \mathbf{C}_\rho| - \frac{n}{2} \log 2\pi \quad (15)$$

For constructing (7) for the non-parametric models we take $\mathbf{M}_0 = \mathbf{C}_\rho^{1/2} (\mathbf{I} - \mathbf{1} \mathbf{1}^\top / n) \mathbf{C}_\rho^{1/2}$ and $\mathbf{M}_1 = \mathbf{C}_\rho^{1/2} (\mathbf{I} - \mathbf{W})^\top (\mathbf{I} - \mathbf{W}) \mathbf{C}_\rho^{1/2}$. Note that matrix \mathbf{M}_1 can be similarly adjusted accordingly for linear models too. In the case of equally spaced data \mathbf{C}_ρ reduces to standard AR(1) correlation structure. In a similar manner as in Section 3.1 and Section 3.2, the p-value $P(F > t_{obs})$ can be calculated as seen in (8). The same principles can be applied in order to adjust the CVF-statistic for the correlated noise assumption. See also Appendix A.2 for a comparison between red noise and white noise Gaussian process regression for simulated light curves with additive red noise.

4 P-value evaluation for generalised F-test

In this section we will refer to more technical details regarding the implementation of the above mentioned tests. Note that the corresponding statistics whose p-values need to be generated, are of the form

$$F = \frac{\hat{\epsilon}^\top \mathcal{A} \hat{\epsilon}}{\hat{\epsilon}^\top \mathcal{B} \hat{\epsilon}}$$

where \mathcal{A} and \mathcal{B} are some symmetric matrices of the same dimension n depending on the model and $\hat{\epsilon}$ represent i.i.d normal error components. The corresponding p-values for some observed value of statistics t_{obs} is therefore

$$P\left(\frac{\hat{\epsilon}^\top \mathcal{A} \hat{\epsilon}}{\hat{\epsilon}^\top \mathcal{B} \hat{\epsilon}} > t_{obs}\right) = P(\hat{\epsilon}^\top (\mathcal{A} - t_{obs} \mathcal{B}) \hat{\epsilon} > 0)$$

Clearly, $\mathcal{A} - \frac{t_{obs}}{c} \mathcal{B}$ is symmetric but not necessarily positive definite, but one could easily see that

$$P(\hat{\epsilon}^\top (\mathcal{A} - t_{obs} \mathcal{B}) \hat{\epsilon} > 0) = P(X = \sum_{i=1}^l \lambda_i \chi_1^2 > 0)$$

Where, λ_i are the $l \leq n$ non-zero eigenvalues, not necessarily positive of $(\mathcal{A} - t_{obs} \mathcal{B})$ and χ_1^2 stands for independent χ^2 random variables with 1 degree of freedom. Note that the matrices \mathcal{A} and \mathcal{B} , when standard linear regression is used, have only two possible eigenvalues: either 0 or 1. This leads to the ratio of two independent chisquare components with $n - m_1$ and $m_1 - m_0$ degrees of freedom respectively which reduces to the standard F distribution (see Butler (2007), p. 378). As the distribution of X is not generally known in the closed form, see Johnson et al. (1995), we need to evaluate these probabilities numerically. There are many methods in the literature for approximating such probabilities, for example numerical integration Imhof (1961) or using the method of matching moments. The moment generating function of the corresponding convolution X is known however and rather than performing the corresponding numerical Laplace inversion, a practically convenient method that we adopt here is that based on the saddlepoint approximation as it is numerically efficient for the accuracy that we need to operate. Moreover, the saddlepoint approximation has been successfully implemented in many timeseries applications e.g. Paolella (2018) and more recently in non euclidean statistics data e.g. Kume et al. (2013). We adopt the methodology that is suggested in Kuonen (1999) as our hypothesis testing methodology is also similar in nature.

4.1 Saddlepoint approximation

Saddlepoint approximation is an approximation method for evaluating a density or a cumulative distribution function given the analytical expression of its moment generating function or the cummulant generating function $\mathcal{K}(\cdot)$ and its derivatives \mathcal{K}' and \mathcal{K}'' , see Butler (2007) for more details. In fact, our focus here is on the CDFs, namely $F(x) = P(X > x)$. Two popular approximations are available for these survival probabilities, as suggested in Lugannani, Rice (1980) and Barndorff-Nielsen (1990). In particular, the approximation of Barndorff-Nielsen (1990) for $\hat{F}(x)$ is derived as

$$\hat{F}(x) = 1 - \Phi\left\{w + \frac{1}{w} \log\left(\frac{u}{w}\right)\right\} \quad (16)$$

where Φ is the standard normal distribution, and w and u are given by, $w = \text{sgn}(\hat{s})[2(\hat{s} - \mathcal{K}(\hat{s}))]^{1/2}$, $u = \hat{s}(\mathcal{K}''(\hat{s}))^{1/2}$. The saddlepoint solution is \hat{s} such that

$$\mathcal{K}'(\hat{s}) = x \quad (17)$$

In our case, we consider the quadratic forms of zero mean normal variables. It can be shown that for some independent random variables, $Z_i \sim N(0, 1)$, the corresponding cumulant generating function of the quadratic form $\sum \lambda_i Z_i^2$ is $\mathcal{K}(s) = -\frac{1}{2} \sum \log(1 - 2s\lambda_i)$ with, $\mathcal{K}'(s) = \sum \frac{\lambda_i}{1-2s\lambda_i}$ and $\mathcal{K}''(s) = \sum \frac{2\lambda_i^2}{(1-2s\lambda_i)^2}$. As can be seen from the expression for \mathcal{K}' , at $s = 1/(2\lambda_i)$ this function is unbounded and therefore the solution of \hat{s} should be carefully chosen. In particular, we have found that the best strategy here is to look for the solution which is the nearest to 0. This implies that the solution of the saddlepoint equation (17) can be also negative. Some examples regarding the accuracy of saddlepoint approximation for our particular problem can be found in Appendix A.1.

5 Power analysis of the tests

In this section we examine the performance of the proposed tests by estimating their power using simulations. The power is the the probability to identify a period as valid when the period is correct, and it is usually denoted as γ . In other words $\gamma = 1 - P(\text{Do not reject } H_0 | H_1 \text{ true})$. The higher the value of the power the better the performance of the test.

5.1 Example 1: Weighted linear regression

We estimate γ using simulated light curves with known periodicity at 2.4 days. We mentioned in Section 3 that in many cases the distribution of the F-statistic (7) no longer follows a standard F distribution. One of these situations is when weighted regression is used. As a first example, we compare the power for the generalized F-test to that of the standard F-test and to the approach described in Thieler et al. (2013) when weighted linear regression is used. For this example $\alpha = 1 - 0.998$. We simulate 1000 sinusoidal light curves with known period consisting of 200 data points for different signal to noise ratios (SNR), $SNR = var(y)/var(\epsilon)$. These light curves will be generated using the package *RobPer* (Thieler et al., 2016). The results are shown in Figure 1 (Left) for the significance level $\alpha = 1 - 0.998$, note that this level is chosen as the multiple tests correction for $\alpha = 0.05$ and 30 repetitions according to Šidák (1967). We notice that the generalised F-test outperforms the other two while closely followed by the standard F-test. Of course the larger the SNR, the larger the power, meaning that the probability of correct inference, which depends on the estimated p-values, gets larger as the SNR increases.

In order to include the testing approach introduced in Thieler et al. (2013), which we denote here as “RThieler”, for each generated light curve we calculated the relevant periodogram for 196 trial periods ranging from 0.5 to 20 and used the *RobPer* package to calculate the relevant critical value. To obtain a clearer view on the test’s performance we further calculate the average number of periods identified as correct, for different signal to noise ratios. In this example we are searching for periods from 0.5 to 10 days with 1 decimal accuracy. Note that the simulated light curves were generated with only one actual period, and thus extra periods detected are false alarms. The results can be seen in Figure 1 (Right), in this plot the number of periods detected should be 1 and thus deviations from that are an indication of poor performance. We can see that the generalized F-test clearly outperforms the other two, with the standard F-test overestimating the number of correct periods and the RThieler test underestimating it. Overall, from this example we can conclude that using the generalized F-test when weighted regression is used can improve the quality of our results compared to the other two methods.

5.2 Example 2: Gaussian process regression

In Section 3.1 and Section 3.2 we discussed that the generalized F and CVF tests can be readily used for more complex models such as Gaussian process regression. In this section we simulate artificial light

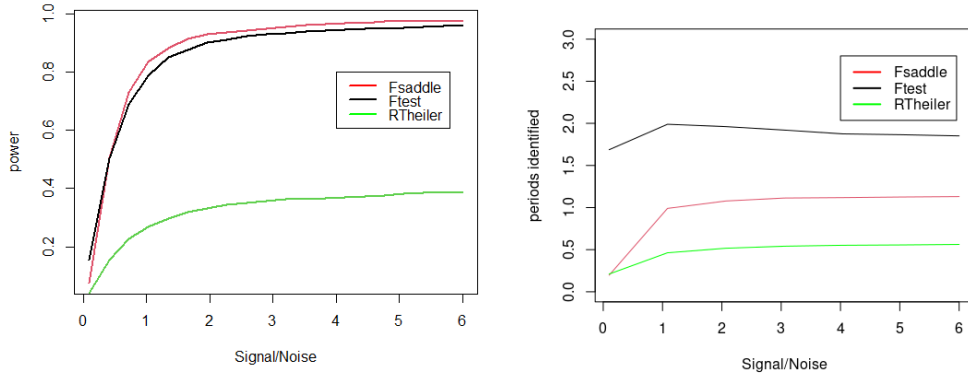


Figure 1: (Left) Comparison of the power between the F-test with Saddlepoint approximation, standard F-test and Theiler’s approach, for different signal to noise ratios. (Right) Comparison between the average number of periods identified as correct for the three tests mentioned. For each value of SNR 1000 curves with 200 data points were generated. The significance level was set to $\alpha = 1 - 0.998$.

curves from a GPR model, fit a Gaussian process regression and perform our tests in order to estimate their power. For this example we borrow the sampling of a randomly selected real light curve (object 3314.I from Froebrich et al. (2021)). We generate our periodic signal from a Gaussian prior using a periodic kernel as in (4) with period at 5.2 days. A typical example of the shape of our simulated data can be seen in Figure 2 (Left). We generate light curves for different signal to noise ratios, ranging from 0.01 to 8. The noise is generated from a zero-mean Normal distribution. We estimate the power for each different value of SNR based on 1000 repetitions. In Figure 2 (Right) we see the power of the generalized F-test at a $1 - \alpha = 99\%$ significance level. We notice that the test performs very well with its power being estimated larger than 0.7 for even SNRs as small as 0.5. For a SNR larger or equal to 1 the power is constantly estimated close to 1.

To our knowledge there doesn’t exist another test under the GPR setting to pose as a comparison. We include in our plot the estimated power of the standard F-test using a sinusoidal model, for the same simulated data, as a reference, acknowledging that the comparison of these tests is not fair. The generalized F-test performs a lot better than the standard F-test in this example as expected. We performed the same analysis for the CVF-test too and obtained very similar results to those obtained from the generalized F-test. In Table 1 we can see a comparison of the power of generalized F and CVF tests for the same simulated data and SNR fixed to 0.65. The power is calculated for different significance levels. Both tests perform very well with their power estimated to be larger than 0.84 for a significance level of $1 - \alpha = 99.5\%$ for example. Of course the larger the $1 - \alpha$ significance level the smaller the estimated power. We should note that the significance levels were chosen as multiple testing corrections according to Šidák (1967) and correspond to different numbers of tests (e.g. 1, 10, 100, 1000) that could be conducted. We notice that the tests behave similarly with the CVF-test having a slightly larger power in this particular example. Finally we also calculated the probability of not rejecting the null hypothesis when the null is true by simulating purely noise data. In all cases the probability was larger or equal to 0.98 for our proposed tests and the same holds for when a linear model and standard F-test is applied.

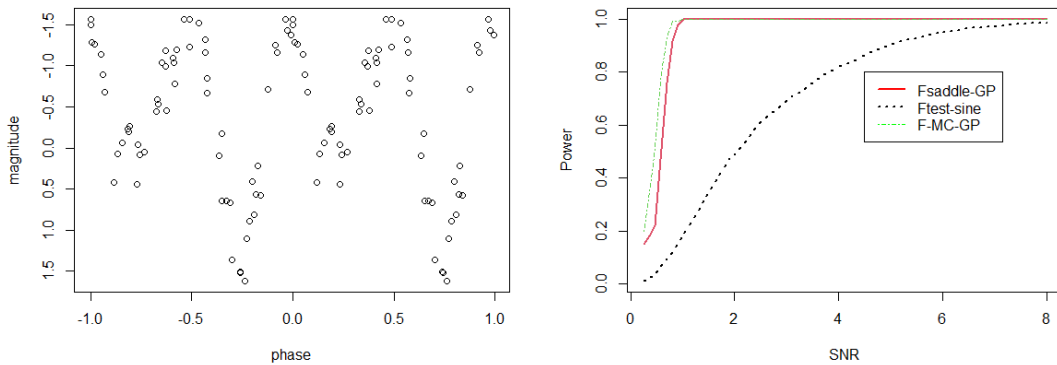


Figure 2: (Left) A phased light curve generated from the GPR model with period 5.2 days with SNR=6. This is a typical example of the shape of the light curves generated. (Right) The estimated power of the GPR generalized F-test of light curves generated for different SNR (red line). the green line shows the power when the same analysis is perform using Monte Carlo and the dashed line shows the power of the standard F-test for a sinusoidal based fitting.

Table 1: This table shows the estimated power of the generalized F and CVF tests for different significance levels.

sig. level	F GPR	CVF GPR
$0.95^{1/1} = 0.95$	0.968	0.970
$0.95^{1/10} = 0.9948838$	0.842	0.848
$0.95^{1/100} = 0.9994872$	0.616	0.612
$0.95^{1/1000} = 0.9999487$	0.352	0.354

6 Application to real light curves

In this section we apply the methodology from the previous sections to real light curves. They are obtained as part of the Hunting Outbursting Young Stars Citizen Science Project (Froeblich et al., 2018). This project combines observational data from professional, university and amateur observatories to construct long-term light curves of young stars. By its very nature the project hence creates in-homogeneously sampled light curves. The example objects investigated here are all situated in the Pelican Nebula, a vast star forming region in Cygnus. Periodic light curves of young stars can be used to measure rotation periods of the stars, as well as to track the evolution of properties of surface features on them.

6.1 Example 1

We first investigate object number 6149 from Froeblich et al. (2021). This object belongs to the population of young stars in the Pelican Nebula and shows a clear periodic behaviour in the four filters B, V, R, and I. The period of the variations has been determined as 2.1763d, from the median of the periods in the individual filters (Froeblich et al., 2021). See Figure 3 where the light curve is plotted for the different filters against time and folded in period 2.1763 days.

We first analyze the light curve independently for each filter, by fitting a weighted Gaussian process model using the periodic kernel and assuming independent residuals. In principle, light curves measured

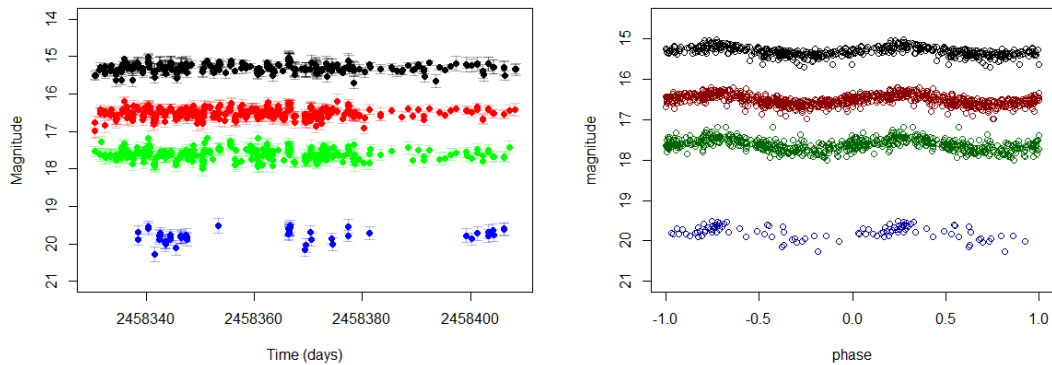


Figure 3: (Left) The light curve number 6149. Each color represents a different filter. Black is for Infrared, red for Red filter, blue for Blue filter and green for Visual. The error bars represent the measurement accuracies. (Right) The light curve number 6149 folded in period 2.1763 days for different filters.

in different filters for the same star should exhibit the same periodic behaviour, so if a method identifies the same period for all filters it is a good sign that the correct period is detected. The periodogram is obtained using F and CVF statistics, see Figure 4 (Left). For this example we search for periods between 0.5 and 30 days with a very rough grid of 1 decimal accuracy. We then apply sequentially the generalized F and CVF tests and identify in most cases the period at 2.2 days as the most important real period. This is the period that corresponds to the maximum F -statistic value and a significant p -value. We notice however, that for some filters the tests identify more than one period as valid and in some cases as in filter R the tests fail to identify any periods. We further run the same analysis but this time assuming some correlation structure for the residuals as described in Section 3.3. We see that with these adjustments the generalized F and CVF tests return as valid only one period at 2.2 days also. It is worth noticing that for filter R the tests identify also the period at 2.2 days.

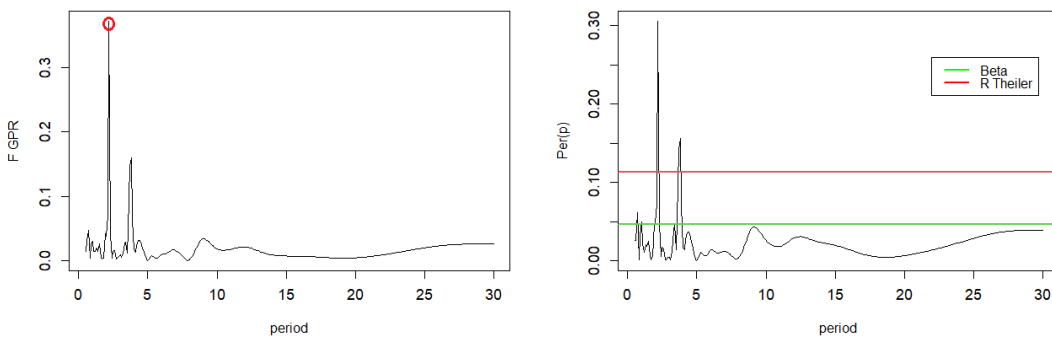


Figure 4: (Left) The weighted GPR F periodogram for light curve 6149 measured in the visual filter. With the red circle we mark the period identified as important according to the generalized F -test. (Right) The weighted least squares sine periodogram for the same light curve. The lines represent the critical values according to the Standard F -test and the “RTheiler” approach, peaks above the lines are considered as important periods.

Next, for comparison, we analyze the lightcurve independently for each filter again, by fitting a sinusoidal wave using weighted least squares regression. We obtain the periodogram based on the R^2 statistic seen in Figure 4 (Right). We then proceed by performing the standard F test and Beta distribution based test as seen in Thiel et al. (2013). The results for all methods and filters are summarized in Table 2. We see that all methods in most cases identify the most important period as 2.2. The standard F test seems to be overestimating the number of valid periods. All methods seem to find as valid other periods than 2.2, with some exceptions for the GPR based tests.

6.2 Example 2

As a second example, we analyze object 3314, measured in filter I and R with a studied period at 13.8783 days, as seen in Froebrich et al. (2021). See Figure 5 (Left) where the light curve is plotted for both filters and Figure 5 (Right) where the light curve is folded in a 13.8783 day period. Similarly to example 1 we apply all previous methods to both filters. The results are summarized in Table 3. We see that for this example all methods behaved in the same way. They all identified only one important period at 13.9 days. In this example the red noise model was applied too returning the same results and was excluded from the table for simplicity.

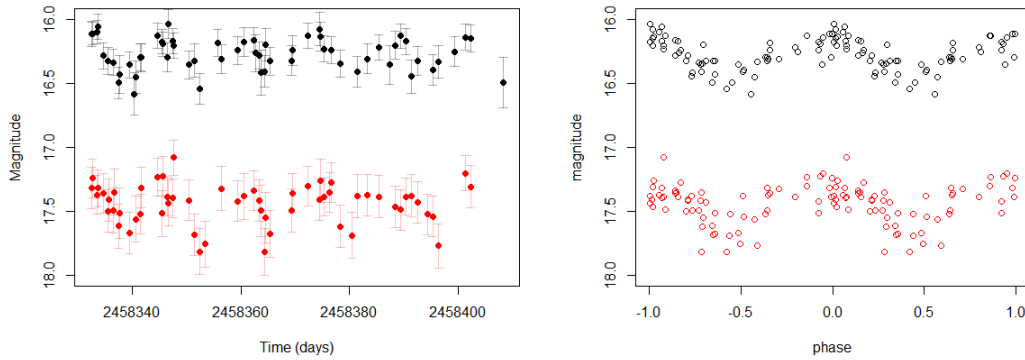


Figure 5: (Left) The light curve number 3314. Black is for Infrared filter and red for Red filter. The error bars represent the measurement accuracies. (Right) The light curve number 3314 folded in period 13.8783 days for different filters.

Table 2: The period identified as most important from the various tests, for different filters. The numbers in the parenthesis denote the number of other periods identified as important from the tests. The dash represents the case that a test did not identify any period as valid.

Filter	F GPR	CVF GPR	F GPR red	CVF GPR red	F sine	Thieler sine
B	2.2 (2 extra)	2.2 (2 extra)	2.2 (0 extra)	2.2 (0 extra)	2.2 (2 extra)	-
R	-	-	2.2 (0 extra)	2.2 (0 extra)	2.2 (3 extra)	2.2 (1 extra)
I	2.2 (1 extra)	2.2 (1 extra)	2.2 (1 extra)	2.2 (1 extra)	2.2 (1 extra)	2.2 (1 extra)
V	2.2 (0 extra)	2.2 (0 extra)	4.3 (1 extra)	4.3 (1 extra)	2.2 (3 extra)	2.2 (1 extra)

Table 3: The period identified as most important from the tests in Example 2, for different R and I. In this case no other period was identified as important from the tests (0 extra periods).

Filter	F GPR	CVF GPR	F sine	Thieler sine
R	13.9 (0 extra)	13.9 (0 extra)	13.9 (0 extra)	13.9 (0 extra)
I	13.9 (0 extra)	13.9 (0 extra)	13.9 (0 extra)	13.9 (0 extra)

6.3 Implementation notes

For the examples in this section we used a rough period grid of one decimal accuracy. This grid is chosen for computational simplicity and it also shows us how methods perform under relatively crude search schemes. In general it is advised to follow the two stage period search method seen in Reimann (1994) and described in Appendix A.2. Another thing to note is that we selected our period grid homogeneously in the range between 0.5 and 30 days. Here we had prior knowledge as to where the potential periods were, since they were studied in Froebrich et al. (2021), and so this approach is sensible as the results also showed. In general applications however, when no prior information is available, it is preferable to select periods in-homogeneously, by building a grid based on the equivalent frequency range instead and ensure that short periods won't be missed.

7 Conclusions and future work

In this paper we provided tests for period detection under non-parametric linear smoother settings, especially Gaussian process regression. The generalized F-statistic is easily and readily adjustable for a range of models. For example it works better than alternative tests when Weighted Least Squares regression is used and the sample size is relatively large. It is also easy to use under ARMA model setting providing more accurate results than asymptotic methods for small sample sizes. The CVF-test statistic based on leave-one-out cross validation for Gaussian process regression behaves similarly to the F. Both statistics can be adjusted for Weighted Gaussian process regression scenarios (when measurement accuracies are available), and also for deviations from white noise. Our simulation results show that adjusting for red noise (when present) leads to more periods correctly identified and smaller number of falsely identified periods. The power of both tests when Gaussian process regression is used is quite high for reasonable signal to noise ratios (e.g. for data with $SNR > 0.6$).

These tests are flexible but there are situations where they cannot be used (e.g L1 regression settings). We have some preliminary results for a test based on bootstrap that can be used under any setting that will be reported as part of a future work. Finally, the methods could be adjusted to take in to account simultaneous measurements from multiple filters. Further research is needed for situations where the data exhibit semi-periodic behaviour. Asymptotic results on the estimator of period under the Gaussian process regression settings could provide useful insights about efficiently calculating periodograms.

Acknowledgements

The authors would like to thank the anonymous referees for improving this paper with their comments.

Data availability statement

The data is available upon request from the authors.

Funding statement

This work was funded by the University of Kent Vice chancellor's scholarship.

References

- Akerlof C, Alcock C, Allsman R, Axelrod T, Bennett DP, Cook KH, Freeman K, Griest K, Marshall S, Park H-S, others* . Application of cubic splines to the spectral analysis of unequally spaced data // *The Astrophysical Journal*. 1994. 436. 787–794.
- Azzalini Adelchi, Bowman Adrian*. On the use of nonparametric regression for checking linear relationships // *Journal of the Royal Statistical Society: Series B (Methodological)*. 1993. 55, 2. 549–557.
- Baltagi Badi H, Wu Ping X*. Unequally spaced panel data regressions with AR (1) disturbances // *Econometric Theory*. 1999. 814–823.
- Barndorff-Nielsen Ole E*. Approximate interval probabilities // *Journal of the Royal Statistical Society: Series B (Methodological)*. 1990. 52, 3. 485–496.
- Benlloch Sara, Wilms Jörn, Edelson Rick, Yaqoob Tahir, Staubert Rüdiger*. Quasi-periodic oscillation in Seyfert galaxies: Significance levels. The case of Markarian 766 // *The Astrophysical Journal Letters*. 2001. 562, 2. L121.
- Berenblut II, Webb GI*. A new test for autocorrelated errors in the linear regression model // *Journal of the Royal Statistical Society: Series B (Methodological)*. 1973. 35, 1. 33–50.
- Bowier J., Matt S. P., Mohanty S., Scholz A., Stassun K. G., Zanni C*. Angular Momentum Evolution of Young Low-Mass Stars and Brown Dwarfs: Observations and Theory // *Protostars and Planets VI*. I 2014. 433.
- Butler Ronald W*. Saddlepoint approximations with applications. 22. 2007.
- Cumming Andrew, Marcy Geoffrey W, Butler R Paul*. The Lick planet search: detectability and mass thresholds // *The Astrophysical Journal*. 1999. 526, 2. 890.
- Do Tuan, Ghez Andrea M, Morris Mark R, Yelda Sylvana, Meyer Leo, Lu Jessica R, Hornstein Seth D, Matthews Keith*. A near-infrared variability study of the galactic black hole: a red noise source with no detected periodicity // *The Astrophysical Journal*. 2009. 691, 2. 1021.
- Durbin James, Watson Geoffrey S*. Testing for serial correlation in least squares regression: I // *Biometrika*. 1950. 37, 3/4. 409–428.
- Froebrich D., Campbell-White J., Scholz A., Eisloffel J., Zegmott T., Billington S. J., Donohoe J., Makin S. V., Hibbert R., Newport R. J., Pickard R., Quinn N., Rodda T., Piehler G., Shelley M., Parkinson S., Wiersema K., Walton I*. A survey for variable young stars with small telescopes: First results from HOYS-CAPS // *Monthly Notices of the Royal Astronomical Society*. VIII 2018. 478, 4. 5091–5103.

- Froeblich Dirk, Derezea Efthymia, Scholz Aleks, Eislöffel Jochen, Vanaverbeke Siegfried, Kume Alfred, Herbert Carys, Campbell-White Justyn, Miller Niall, Stecklum Bringfried, others* . A survey for variable young stars with small telescopes–IV. Rotation periods of YSOs in IC 5070 // *Monthly Notices of the Royal Astronomical Society*. 2021. 506, 4. 5989–6000.
- Hall Peter, Reimann James, Rice John*. Nonparametric estimation of a periodic function // *Biometrika*. 2000. 87, 3. 545–557.
- Halpern Jules P, Leighly KM, Marshall HL*. An extreme ultraviolet explorer atlas of seyfert galaxy light curves: Search for periodicity // *The Astrophysical Journal*. 2003. 585, 2. 665.
- Hamilton James Douglas*. Time series analysis. 2020.
- Heerah Sachin, Molinari Roberto, Guerrier Stéphane, Marshall-Colón Amy*. Granger-Causal Testing for Irregularly Sampled Time Series with Application to Nitrogen Signaling in Arabidopsis // *bioRxiv*. 2020.
- Herbst W., Eislöffel J., Mundt R., Scholz A*. The Rotation of Young Low-Mass Stars and Brown Dwarfs // *Protostars and Planets V. I* 2007. 297.
- Imhof Jean-Pierre*. Computing the distribution of quadratic forms in normal variables // *Biometrika*. 1961. 48, 3/4. 419–426.
- Johnson Norman L, Kotz Samuel, Balakrishnan Narayanaswamy*. Continuous univariate distributions, volume 2. 289. 1995.
- Katkovnik Vladimir*. Robust M-periodogram // *IEEE Transactions on Signal processing*. 1998. 46, 11. 3104–3109.
- Kume Alfred, Preston Simon P, Wood Andrew TA*. Saddlepoint approximations for the normalizing constant of Fisher–Bingham distributions on products of spheres and Stiefel manifolds // *Biometrika*. 2013. 100, 4. 971–984.
- Kuonen Diego*. Miscellanea. Saddlepoint approximations for distributions of quadratic forms in normal variables // *Biometrika*. 1999. 86, 4. 929–935.
- Lomb Nicholas R*. Least-squares frequency analysis of unequally spaced data // *Astrophysics and space science*. 1976. 39, 2. 447–462.
- Lugannani Robert, Rice Stephen*. Saddle point approximation for the distribution of the sum of independent random variables // *Advances in applied probability*. 1980. 12, 2. 475–490.
- Oh Hee-Seok, Nychka Doug, Brown Tim, Charbonneau Paul*. Period analysis of variable stars by robust smoothing // *Journal of the Royal Statistical Society: Series C (Applied Statistics)*. 2004. 53, 1. 15–30.
- Paolella Marc S*. Linear models and time-series analysis: regression, ANOVA, ARMA and GARCH. 2018.
- Reimann James Dennis*. Frequency estimation using unequally-spaced astronomical data. 1994.
- Scargle Jeffrey D*. Studies in astronomical time series analysis. II-Statistical aspects of spectral analysis of unevenly spaced data // *The Astrophysical Journal*. 1982. 263. 835–853.
- Schulz Michael, Statterger Karl*. SPECTRUM: Spectral analysis of unevenly spaced paleoclimatic time series // *Computers & Geosciences*. 1997. 23, 9. 929–945.

- Schuster Arthur*. On the investigation of hidden periodicities with application to a supposed 26 day period of meteorological phenomena // *Terrestrial Magnetism*. 1898. 3, 1. 13–41.
- Schwarzenberg-Czerny A*. The distribution of empirical periodograms: Lomb-Scargle and PDM spectra // *Monthly Notices of the Royal Astronomical Society*. 1998. 301, 3. 831–840.
- Šidák Zbyněk*. Rectangular confidence regions for the means of multivariate normal distributions // *Journal of the American Statistical Association*. 1967. 62, 318. 626–633.
- Thieler Anita M, Fried Roland, Rathjens Jonathan, others* . RobPer: An R Package to Calculate Periodograms for Light Curves Based on Robust Regression // *Journal of Statistical Software*. 2016. 69, 9. 1–36.
- Thieler Anita Monika, Backes Michael, Fried Roland, Rhode Wolfgang*. Periodicity detection in irregularly sampled light curves by robust regression and outlier detection // *Statistical Analysis and Data Mining: The ASA Data Science Journal*. 2013. 6, 1. 73–89.
- VanderPlas Jacob T*. Understanding the lomb–scargle periodogram // *The Astrophysical Journal Supplement Series*. 2018. 236, 1. 16.
- VanderPlas Jacob T, Ivezić Željko*. Periodograms for multiband astronomical time series // *The Astrophysical Journal*. 2015. 812, 1. 18.
- Vaughan S*. A simple test for periodic signals in red noise // *Astronomy & Astrophysics*. 2005. 431, 1. 391–403.
- Von Storch Hans, Zwiers Francis W*. *Statistical analysis in climate research*. 2001.
- Wang Yuyang, Khardon Roni, Protopapas Pavlos*. Nonparametric bayesian estimation of periodic light curves // *The Astrophysical Journal*. 2012. 756, 1. 67.
- Williams Christopher KI, Rasmussen Carl Edward*. *Gaussian processes for machine learning*. 2, 3. 2006.
- Zhou Wei-Xing, Sornette Didier*. Statistical significance of periodicity and log-periodicity with heavy-tailed correlated noise // *International Journal of Modern Physics C*. 2002. 13, 02. 137–169.

A Appendix

A.1 Exploring the Saddlepoint approximation accuracy

In this subsection we will see some numerical examples in order to understand further the behaviour of the Saddlepoint approximation for the statistics proposed in this paper. We will start by approximating the cumulative distribution function (CDF) of the generalized F-statistic under the null hypothesis when the alternative is a periodic Gaussian process model.

In order to examine the performance of Saddlepoint approximation, we simulate 10000 values of the generalized F-statistic under the null hypothesis assumption and calculate its empirical cumulative distribution function (ECDF), which we compare with the CDF obtained by using Saddlepoint, see Figure 6 (Left). Saddlepoint approximation gives results that are very close to the empirical CDF of the statistic. In addition, we plot the CDF approximated using numerical integration according to Imhof (1961) getting almost the same results with the other approaches. The only difference is that Saddlepoint approximation

Table 4: Time in seconds for 50 repetitions of the different methods.

	Saddlepoint	Imhof	Monte Carlo	Exact
GPR	16.30	17.56	774.90	–
OLS	0.79	1.24	4.10	0.02

is faster, see more details at Table 4 for a time comparison between the methods. Please note that whenever we report ECDF values below we mean the empirical CDF of 10000 replications. Similar results have been produced for the saddlepoint approximation of the CVF-statistic. In Figure 6 (Right) we see that the saddlepoint approximation of CVF under the null when GPR is used as the alternative also works well.

The hypothesis testing proposed can be also used to model correlated background noise and in many cases can perform better than standard asymptotic tests. In this example we will compare the approximations of the CDF of the F-statistic under the presence of AR(1) type noise and when the alternative is fitting a sinusoidal model. Under this scenario the standard F-statistic can no longer be assumed to follow an $F(m_1 - m_0, n - m_1)$ distribution, but there is an asymptotic result (Hamilton (2020)) based on Chi-square distribution with $m_1 - m_0$ degrees of freedom. In Figure 7 we compare the approximations of the CDF of the F-statistic for two different scenarios based on the sample size. For a relatively big sample size of 200 data points both the Saddlepoint approximation and the asymptotic result are close to the empirical CDF. When the sample size gets small however, as in Figure 7 (Right) with 20 data points, the asymptotic result based on chi square no longer works well. The Saddlepoint on the other hand still approximates the distribution quite accurately.

Finally, in Section 4 we discussed an optimal way in order to find a solution to the saddlepoint equation (17). An example of the general behaviour of \mathcal{K}' can be seen in Figure 8.

A.2 Red noise vs White noise GPR model

In Section 3.3 we saw how our test statistics F and CVF can be adjusted when our data are contaminated with red noise. Adjusting the models and tests to the correct noise assumption can improve drastically our results. More specifically, assuming a white noise model when the residuals are correlated can lead to periods failing to be identified and also to an increased number of falsely detected periods. As an example we will generate 100 light curves for 3 different correlated noise scenarios ($\rho = 0.1, 0.5, 0.9$) with variance 1. The curves will be generated from a Gaussian process prior with a periodic kernel and period at 5.1 days. The mean behaviour of the curves will be fixed for all curves in all scenarios and it will be a realisation from the Gaussian process prior. We will borrow the sampling times from a real light curve (object 6785.I from Froebrich et al. (2021)). A typical example of the simulated data used here can be seen in Figure 9. Note that the performance of the methods is not affected by the magnitude’s scale.

For these simulated light curves we will fit a Gaussian process regression model with a correlation structure \mathbf{C}_ρ for AR(1) residuals. For this example, we estimate the parameters by minimizing the equivalent squared leave-one-out cross-validation error. We will search for potential periods between 1 and 10 days with 1 decimal accuracy. Note that this particular period search grid is chosen for computational convenience. For real applications it is preferable to use the two-stage grid search method as seen in Wang et al. (2012) and Reimann (1994), whereby some N periods are initially chosen corresponding to the top N periodogram peaks based on a rough period grid, and then a finer period search grid is applied around each of the N chosen periods from the previous step. The results obtained by the red noise model will also be compared to those from the standard GPR model. We notice that for all three scenarios the red noise GPR model most of the time has the maximum peak of the F-statistic periodogram at the correct period, on the other hand, the white noise model (standard GPR) most of the time fails to do so. These results

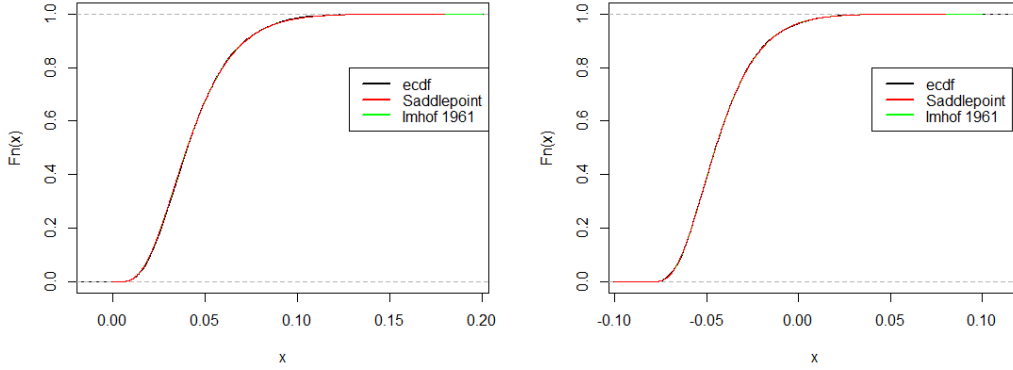


Figure 6: (Left) An example of the ECDF and the saddlepoint approximation of the corresponding generalized F-statistic based on the RSS of White Noise and GPR models. The green line that agrees with the saddlepoint approximation is the approximation based on the numerical integration method. (Right) The same comparison of methods for the CVF-statistic of GPR.

are summarized in Table 5 under the columns labelled as “correct peak”.

Furthermore, we apply the generalized F-test as described in Section 3 to all simulated curves for a significance level $1 - \alpha$ set to $0.95^{1/91} = 0.9994365$. This is the correction for multiple tests as seen in Šidák (1967), 91 is the number of tests conducted which is the number of trial periods in our case. Almost always the correct period (at 5.1 days) was identified as significant (more than 99% of the time). When the wrong model (white noise) was used however, we had an increased number of false period discoveries compared to that of using the red noise GPR model. Specifically, after performing our period detection test, in many cases other periods, except for the true one, appeared to be falsely significant. These results are summarized in Table 5 under the columns labelled as “false periods”, where we show the average number of periods falsely appearing to be significant, for each simulation scenario.

A.3 Power comparison - Second example

Here we show another example similar to that shown in Section 5.2. For this example we borrow the sampling of a randomly selected real light curve (object 3314_I from Froebrich et al. (2021)). We generate our periodic signal from a Gaussian prior using a periodic kernel as in (4) with period at 5.2 days. A

Table 5: A comparison between the red and white noise Gaussian process regression models fitted to red noise data. The columns labelled “correct peak” show the percentage of the periodograms that had the maximum peak at correct period $p = 5.1$. The columns labelled “false periods” show the average number of periods falsely identified as valid.

ρ	GPR red noise		GPR white noise	
	correct peak	false periods	correct peak	false periods
0.1	90%	1.34	33%	3.56
0.5	79%	0.88	25%	3.62
0.9	84%	1.20	44%	2.90

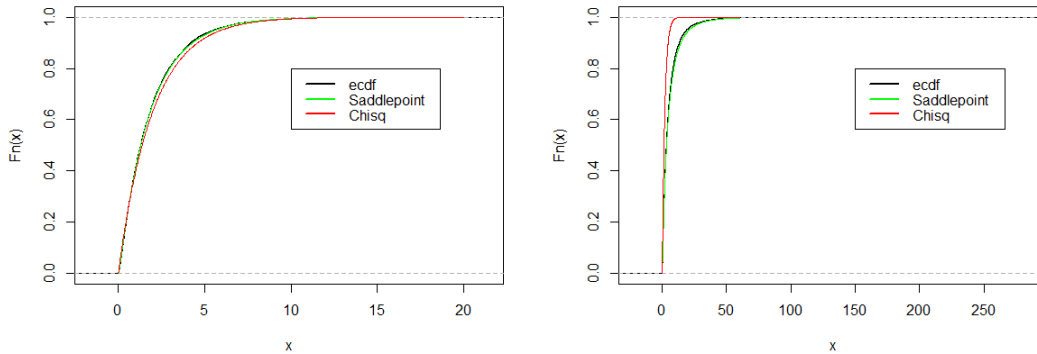


Figure 7: (Left) A comparison of the CDF of the F-statistic under the null of correlated noise for a light curve of 200 observations. The black line shows the empirical CDF, the green line corresponds to Saddlepoint approximation and the red line is the asymptotic Chisquare distribution. (Right) A comparison of the CDF of F-statistic under the null of correlated noise for a light curve of 200 observations. Note that when the sample size is very small the asymptotic result no longer holds but the saddlepoint method approximated the CDF quite accurately.

typical example of the shape of our simulated data can be seen in Figure 10 (Left). We generate light curves for different signal to noise ratios, ranging from 0.01 to 6. The noise is generated from a zero-mean Normal distribution. We estimate the power for each different value of SNR based on 1000 repetitions. In Figure 10 (Right) we see the power of the generalized F-test at a $1 - \alpha = 99\%$ significance level. We notice that the test performs very well with its power being estimated larger than 0.7 for even SNRs as small as 0.5. For a SNR larger or equal to 1 the power is constantly estimated close to 1.

We include in our plot the estimated power of the standard F-test using a sinusoidal model, for the same simulated data, as a reference. The tests in this example seem to perform similarly in terms of power with the generalized F-test being better. We performed the same analysis for the CVF-test too and obtained very similar results to those obtained from the generalized F-test. In Table 1 we can see a comparison of the power of generalized F and CVF tests for the same simulated data and SNR fixed to 0.65. The power is calculated for different significance levels. Both tests perform very well with their power estimated to be larger than 0.92 for a significance level of $1 - \alpha = 99.5\%$ for example. Of course the larger the $1 - \alpha$ significance level the smaller the estimated power. We notice that the tests behave similarly with the CVF-test having a slightly larger power in this particular example.

Table 6: This table shows the estimated power of the generalized F and CVF tests for different significance levels.

sig. level	F GPR	CVF GPR
$0.95^{1/1} = 0.95$	0.987	0.987
$0.95^{1/10} = 0.9948838$	0.922	0.924
$0.95^{1/100} = 0.9994872$	0.714	0.715
$0.95^{1/1000} = 0.9999487$	0.439	0.446

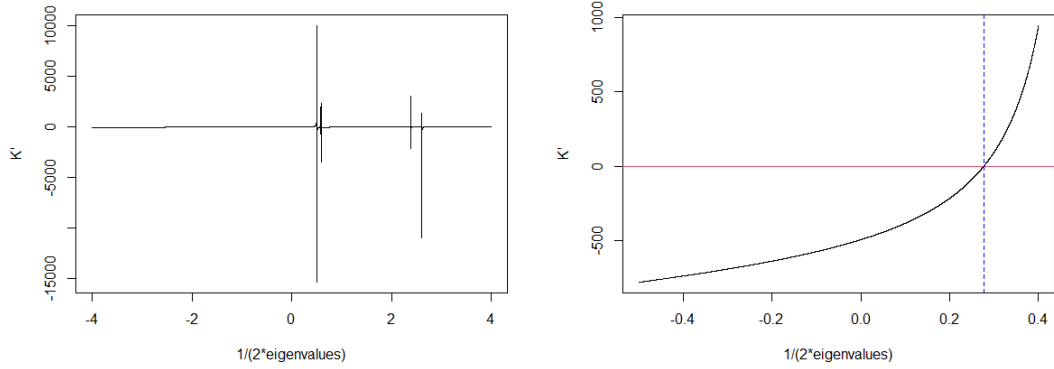


Figure 8: (Left) An example of the \mathcal{K}' function, we see that its behaviour can be quite problematic making the choice of a suitable range to search for the solution important. (Right) For the same example only the range from the biggest negative to the smallest positive. The blue dashed line shows the solution of the Saddlepoint equation which in this case is 0.2763643.

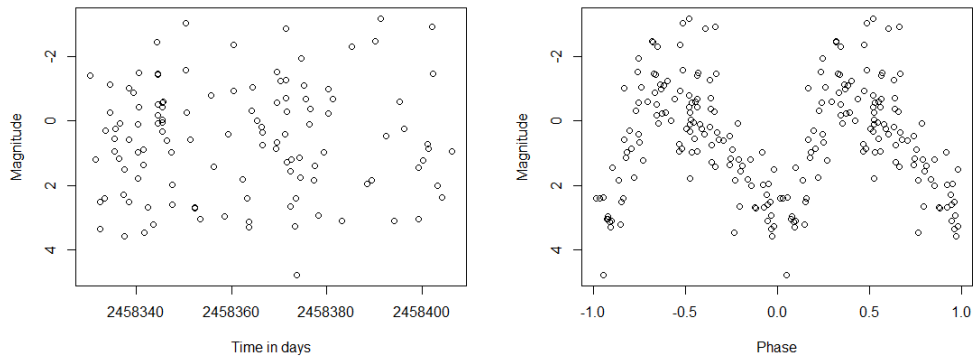


Figure 9: (Left) Simulated light curve from GPR prior with period at 5.1 days. The sampling is borrowed from a real light curve and this shape is used throughout the example of Table 1. (Right) the same simulated light curve folded into period of 5.1 days.

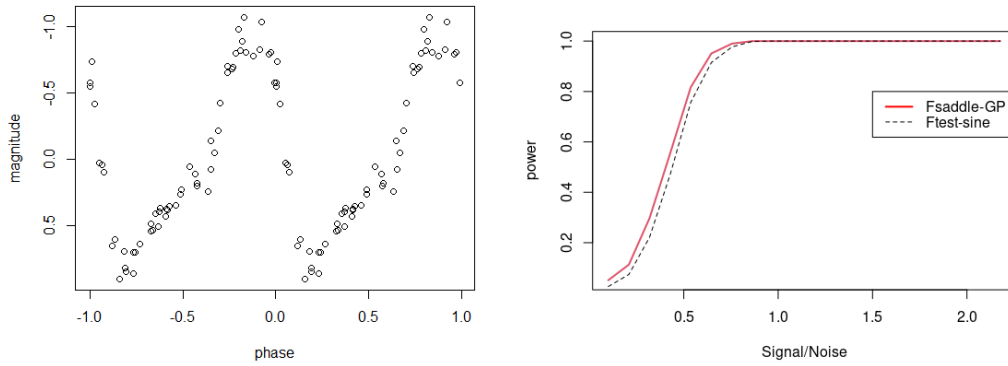


Figure 10: (Left) A phased light curve generated from the GPR model with period 5.2 days with SNR=6. This is a typical example of the shape of the light curves generated. (Right) The estimated power of the GPR generalized F-test of light curves generated for different SNR (red line). The dashed line shows the power of the standard F-test for a sinusoidal based fitting.